A&A 465, 1041–1049 (2007)
DOI: 10.1051/0004-6361:20066636

Astronomy & Astrophysics

Radiative transfer in cylindrical threads with incident radiation

IV. Time-dependent and thermal equilibrium models

P. Gouttebroze

Institut d'Astrophysique Spatiale, Univ. Paris XI/CNRS, Bât. 121, 91405 Orsay Cedex, France
e-mail: pierre.gouttebroze@ias.u-psud.fr

Received 25 October 2006 / Accepted 2 January 2007

ABSTRACT

Context. Relatively cool and dense structures embedded in the solar corona (filaments, prominences, spicules, etc.) may be observed in hydrogen lines. Sometimes they last during several solar rotations.
Aims. Our goal is to evaluate the lifetime of cool structures of the solar corona, determine their evolution from given physical conditions, and compute models in thermal equilibrium.
Methods. We use numerical methods to simultaneously solve the equations of NLTE radiative transfer, statistical equilibrium of hydrogen level populations, and electric neutrality. Radiative transfer equations are solved using cylindrical coordinates and prescribed solar incident radiations. The computation of internal energy and radiative losses and gains yields the rates of temperature evolution.
Results. For isothermal-isobaric cylinders with prescribed physical conditions, we determine the lifetimes and evolution rates for different positions along the radius. For models with prescribed diameter and pressure, we determine the run of temperature vs. radius corresponding to thermal equilibrium. This equilibrium is found to be stable for the whole range of parameters under investigation.
Conclusions. The cores of large and high-pressure cylinders are found to evolve very slowly. This opens the possibility of observing these cool structures at temperatures somewhat different from that corresponding to theoretical radiative equilibrium.

Key words. methods: numerical – radiative transfer – Sun: corona – Sun: filaments – Sun: prominences

1. Introduction

Flux tubes, with different sizes, densities, and temperatures, appear to be the basic components of the outer solar atmosphere: chromosphere, corona, and transition region. This kind of quasi-cylindrical structures may be invoked for the modeling of different solar features: coronal loops, spicules, and prominence threads. Moreover, the chromosphere observed in the hydrogen Lyman-α line at high angular resolution (Bonnet et al. 1980; Vourlidas et al. 2001) looks like a forest of small flux tubes. To properly model these objects, we have developed specific methods to solve numerically radiative transfer equations in cylindrical geometry. The three preceding papers of this series were dedicated to the determination of intensities emitted by the solar plasma contained in cylindrical enclosures, once the internal physical conditions (temperature, pressure) are known. In this way, they aimed at the diagnostic problem. Paper I (Gouttebroze 2004) was restricted to the one-dimensional (radial) problem, while Papers II and III (Gouttebroze 2005, 2006) investigated the two-dimensional (radius- and azimuth-dependent) problem.

The scope of the present paper is somewhat different and concerns the thermal evolution and equilibrium of cylindrical structures. In the absence of internal energy sources, matter inside flux tubes should be close to radiative equilibrium, to have a lifetime long enough to be observed.

The solution of radiative equilibrium equations is one of the fundamental problems of the radiative transfer theory. In particular, the determination of the temperature variation in the outer layers of the star is probably the most ancient problem studied in this field (see, e.g., Milne 1921 or Hopf 1934). These early analytical works were restricted to LTE and grey approximations. Later on, with the development of computers, more realistic problems were solved numerically. Non-grey LTE (e.g., Mihalas 1967) and non-grey NLTE (e.g., Auer & Mihalas 1969; Anderson 1989) problems were successively treated. Concerning isolated structures imbedded in the solar corona, Heasley & Mihalas (1976) computed models of prominences in radiative equilibrium, in the plane-parallel approximation. The case of small planar structures, with combined radiative and conductive energy balance, was subsequently studied by Fontenla & Rovira (1983, 1985).

In the present paper, we return to the one-dimension (vertical) model of Paper I. General formulae are given in Sect. 2. Section 3 concerns the lifetime of isothermal isobaric models in the absence of internal energy sources. In Sect. 4, we study the temporal evolution of structures assuming a quasi-static statistical equilibrium. The final state of structures determines a radiative equilibrium (RE) model. We discuss the temperature structures of these RE models as a function of their pressure and diameter, and examine their stability.

2. Formulation

As in Paper I, we consider a cylinder with a vertical axis, filled with a mixture of hydrogen and helium, with the proportion of one atom of helium to ten atoms of hydrogen. Helium is assumed to be neutral and its contribution to opacity is neglected. The boundary conditions for the solution of radiative transfer equations are provided by the intensities observed over the solar surface, multiplied by dilution factors depending on the altitude and frequency-dependent limb-darkening functions (for details, see Paper I). The models in Sects. 3 and 4 satisfy the equations of radiative transfer, statistical equilibrium of hydrogen level

populations, and electric neutrality. In addition, the models in Sect. 4 satisfy the radiative equilibrium equations.

2.1. List of symbols

Most symbols used in this paper are usual. However, to avoid possible confusion (for instance between quantities given per unit mass and their equivalent per unit volume) it is better to give the full list here, as follows:
$A_{\rm He}$: abundance factor $N_{\rm He}/N_{\rm H}$ (fixed to 0.1);
A_{ji}, B_{ij}, B_{ji}: Einstein coefficients for spontaneous emission, absorption, and stimulated emission, respectively;
C_{ij}: collisional transition rate per atom;
c: velocity of light;
c, as index: relative to the continuum level (e.g. n_c);
D: external diameter of the cylinder;
$E_{\rm rad}$: net gain of energy, per unit mass and time;
g_i: statistical weight of level i;
H: altitude over the solar surface;
h: Planck constant;
I_ν: specific intensity at frequency ν;
$J_\nu = \oint I_\nu {\rm d}\Omega/4\pi$: angle-averaged intensity;
k: Boltzmann constant;
L: number of discrete levels of the hydrogen atom;
$m_{\rm e}$: mass of electron;
$m_{\rm H}$: mass of hydrogen atom;
$m_{\rm He}$: mass of helium atom;
$N_{\rm e}$: number density of electrons;
$N_{\rm H}$: number density of hydrogen (neutral or ionized);
$N_{\rm He}$: number density of helium;
$n_{\rm e} = N_{\rm e}/\rho$: number of electrons per unit mass;
$n_{\rm H} = N_{\rm H}/\rho$: number of hydrogen atoms per unit mass;
n_j: number of hydrogen atoms at level j, per unit mass;
P: gas pressure;
P_{ij}: transition rate per atom from level i to level j;
r: radial coordinate;
$S_\nu = \epsilon_\nu/\kappa_\nu$: source function;
T: temperature;
t: time;
$t_{\rm CP}$: characteristic relaxation time at constant pressure;
$t_{\rm CV}$: characteristic relaxation time at constant volume;
U: internal energy per unit mass;
$U_{\rm exc}$: excitation energy;
$U_{\rm ion}$: ionization energy;
$y = N_{\rm e}/N_{\rm H} = n_{\rm e}/n_{\rm H}$: ionization ratio;
α_ν: photoionization cross section at frequency ν;
Δt: time interval;
ϵ_ν: emission coefficient per unit volume;
κ_ν: absorption coefficient per unit path length;
ν: frequency;
ν_{ij}: frequency difference between levels i and j;
$\nu_{\rm ic}$: frequency difference between level i and continuum;
ξ: microturbulent velocity (fixed to 5 km s^{-1});
ρ: density;
ϕ_ν: normalized absorption profile.
A dot over a symbol indicates a time derivative (e.g. $\dot{y} = {\rm d}y/{\rm d}t$).

2.2. Internal energy and state equation

Once the chemical composition is defined, the number of hydrogen atoms per unit mass is fixed to

$$n_{\rm H} = \frac{1}{m_{\rm H} + A_{\rm He} m_{\rm He}}. \quad (1)$$

The internal energy is the sum of kinetic, ionization, and excitation energies, kinetic energy including the contributions of hydrogen, helium, and electrons, which gives

$$U = \frac{3}{2} n_{\rm H} (1 + A_{\rm He} + y)\, kT + U_{\rm ion} + U_{\rm exc} \quad (2)$$

with

$$U_{\rm ion} = n_{\rm H} h\nu_{1c}\, y \quad (3)$$

and

$$U_{\rm exc} = \sum_{j=1}^{L} h\nu_{1j}\, n_j. \quad (4)$$

Since all electrons come from hydrogen ionization, the electron and proton densities are equal, and the principle of electric neutrality gives

$$n_{\rm H} = \sum_{j=1}^{L} n_j + n_{\rm e}. \quad (5)$$

In a similar way, the pressure may be written:

$$P = (N_{\rm H} + N_{\rm He} + N_{\rm e})\, kT = \rho\, n_{\rm H} (1 + A_{\rm He} + y)\, kT. \quad (6)$$

2.3. Radiative gains and losses

The radiative losses of energy by emission, per unit *volume* and time, in the frequency interval dν are $\epsilon_\nu {\rm d}\nu = \kappa_\nu S_\nu {\rm d}\nu$, and the radiative gains by absorption $\kappa_\nu J_\nu {\rm d}\nu$. So, the net gain of energy by radiation, per unit *mass* and time, over the whole spectrum, is

$$E_{\rm rad} = \frac{1}{\rho} \int_0^\infty \kappa_\nu (J_\nu - S_\nu)\, {\rm d}\nu. \quad (7)$$

Hydrogen being the only active element, contributions to $E_{\rm rad}$ are calculated separately for each line and each bound-free transition of this element, and subsequently added together. The absorption coefficients κ_ν and the source functions S_ν depend on the level populations of the hydrogen atom. Intensities J_ν are computed by solving NLTE radiative transfer equations in cylindrical geometry, with appropriate boundary conditions, as described in Paper I. For a hydrogen model atom with L discrete levels and one continuum, the computation will include $L(L-1)/2$ lines and L bound-free transitions. In the following, L is set to 5, unless stated otherwise.

2.4. Rate equations

The variations of atomic level populations are, for $i \le L$,

$$\frac{{\rm d}n_i}{{\rm d}t} = \sum_{j=1}^{L} \left(n_j P_{ji} - n_i P_{ij} \right) + n_{\rm c} P_{{\rm c}i} - n_i P_{{\rm i c}} \quad (8)$$

(with $P_{jj} = 0$). Similarly, the variation of population for the continuum level is

$$\frac{{\rm d}n_{\rm e}}{{\rm d}t} = \frac{{\rm d}n_{\rm c}}{{\rm d}t} = \sum_{j=1}^{L} \left(n_j P_{{\rm j c}} - n_{\rm c} P_{{\rm c}j} \right). \quad (9)$$

When statistical equilibrium is satisfied, both ${\rm d}n_i/{\rm d}t$ and ${\rm d}n_{\rm e}/{\rm d}t$ vanish. Each transition rate P_{ij} is the sum of a collisional term, depending on electron density and temperature, and a radiative

term depending on the intensity J_ν. So, the evaluation of P_{ij} first requires the solution of radiative transfer equations. For a discrete transition with $j > i$,we have

$$P_{ij} = C_{ij} + B_{ij} \int_{\rm line} J_\nu \phi_\nu {\rm d}\nu \tag{10}$$

and

$$P_{ji} = C_{ji} + A_{ji} + B_{ji} \int_{\rm line} J_\nu \phi_\nu {\rm d}\nu \tag{11}$$

and, for a bound-free transition,

$$P_{ic} = C_{ic} + 4\pi \int_{\nu_{ic}}^{\infty} \frac{\alpha_\nu}{h\nu} J_\nu {\rm d}\nu \tag{12}$$

and

$$P_{ci} = C_{ci} + N_{\rm e} \Phi_{ic}(T) 4\pi \int_{\nu_{ic}}^{\infty} \frac{\alpha_\nu}{h\nu} \left(\frac{2h\nu^3}{c^2} + J_\nu \right) {\rm e}^{-h\nu/kT} {\rm d}\nu \tag{13}$$

with

$$\Phi_{ic}(T) = \frac{g_i}{2g_{\rm c}} \left(\frac{h^2}{2\pi m_{\rm e} kT} \right)^{3/2} {\rm e}^{h\nu_{ic}/kT}. \tag{14}$$

From the rates of variation of level populations, we can deduce the time derivative of the ionization ratio

$$\dot{y} = \frac{1}{n_{\rm H}} \frac{{\rm d}n_{\rm e}}{{\rm d}t}. \tag{15}$$

Differentiating Eq. (3) and combining it with Eqs. (9) and (15), we obtain the variations of internal energy related to ionization

$$\dot{U}_{\rm ion} = h\nu_{1{\rm c}} \sum_{j=1}^{L} \left(n_j P_{j{\rm c}} - n_{\rm c} P_{{\rm c}j} \right). \tag{16}$$

Similarly, Eqs. (4) and (8) yield

$$\dot{U}_{\rm exc} = \sum_{i=1}^{L} h\nu_{1i} \left[\sum_{j=1}^{L} \left(n_j P_{ji} - n_i P_{ij} \right) + n_{\rm c} P_{ci} - n_i P_{ic} \right]. \tag{17}$$

The temporal variation of internal energy is, from Eq. (2),

$$\frac{{\rm d}U}{{\rm d}t} = \frac{3}{2} n_{\rm H} kT\, \dot{y} + \frac{3}{2} n_{\rm H} (1 + A_{\rm He} + y) k \frac{{\rm d}T}{{\rm d}t} + \dot{U}_{\rm ion} + \dot{U}_{\rm exc} \tag{18}$$

and the differentiation of Eq. (6) yields

$$\frac{{\rm d}\ln P}{{\rm d}t} = \frac{{\rm d}\ln \rho}{{\rm d}t} + \frac{\dot{y}}{1 + A_{\rm He} + y} + \frac{{\rm d}\ln T}{{\rm d}t}. \tag{19}$$

2.5. Radiative relaxation

If there is no source of energy inside the cylinder, the change of internal energy is, according to the first law of thermodynamics,

$$\frac{{\rm d}U}{{\rm d}t} = E_{\rm rad} + \frac{P}{\rho^2} \frac{{\rm d}\rho}{{\rm d}t}. \tag{20}$$

We may define a characteristic relaxation time (CRT) as the ratio $U/|{\rm d}U/{\rm d}t|$. It indicates whether the system is close to equilibrium or not and gives an order of magnitude concerning the lifetime of the system. As U and ${\rm d}U/{\rm d}t$, it is a function of the radial coordinate r. Equations (18) and (20) govern the evolution of the system, provided that a further constraint on thermodynamical variables is given, to close the system of equations. We investigate two different possibilities: constant volume and constant pressure.

2.6. System evolution at constant volume

In this case, Eq. (20) reduces to

$$\left(\frac{{\rm d}U}{{\rm d}t} \right)_V = E_{\rm rad} \tag{21}$$

so that the CRT is simply

$$t_{\rm CV} = \frac{U}{|E_{\rm rad}|}, \tag{22}$$

U being given by Eqs. (2) to (4). The time derivative of temperature follows, from Eq. (18), as

$$\left(\frac{{\rm d}T}{{\rm d}t} \right)_V = \frac{E_{\rm rad} - \frac{3}{2} n_{\rm H} kT \dot{y} - \dot{U}_{\rm ion} - \dot{U}_{\rm exc}}{\frac{3}{2} n_{\rm H} (1 + A_{\rm He} + y) k}. \tag{23}$$

2.7. System evolution at constant pressure

According to Eq. (19), the condition of constant pressure is

$$\frac{1}{\rho} \frac{{\rm d}\rho}{{\rm d}t} + \frac{\dot{y}}{1 + A_{\rm He} + y} + \frac{1}{T} \frac{{\rm d}T}{{\rm d}t} = 0. \tag{24}$$

This relation is used to eliminate ${\rm d}\rho/{\rm d}t$ in Eq. (20). With the help of Eqs. (18) and (6), we obtain the temperature derivative

$$\left(\frac{{\rm d}T}{{\rm d}t} \right)_P = \frac{E_{\rm rad} - \frac{5}{2} n_{\rm H} kT \dot{y} - \dot{U}_{\rm ion} - \dot{U}_{\rm exc}}{\frac{5}{2} n_{\rm H} (1 + A_{\rm He} + y) k}. \tag{25}$$

This expression may be substituted into Eq. (18) to yield

$$\left(\frac{{\rm d}U}{{\rm d}t} \right)_P = \frac{3}{5} E_{\rm rad} + \frac{2}{5} \left(\dot{U}_{\rm ion} + \dot{U}_{\rm exc} \right), \tag{26}$$

so that the CRT at constant pressure is

$$t_{\rm CP} = \frac{U}{|\frac{3}{5} E_{\rm rad} + \frac{2}{5} \left(\dot{U}_{\rm ion} + \dot{U}_{\rm exc} \right)|}. \tag{27}$$

In the case when statistical equilibrium (SE) is satisfied, $\dot{U}_{\rm ion}$ and $\dot{U}_{\rm exc}$ vanish, which yields a simple relation between the two characteristic times

$$(t_{\rm CP})_{\rm SE} = \frac{5}{3} t_{\rm CV}. \tag{28}$$

3. Isothermal and isobaric models

These models are defined by the following parameters: temperature T, gas pressure P, external diameter D, and altitude H above the solar surface. The microturbulent velocity ξ, which is a parameter of secondary importance (except for line profiles), is set to 5 km s^{-1} all along the computations. Other parameters, such as the density ρ or the electron density $N_{\rm e}$ are determined by the solution of the system of equations, including state equation, radiative transfer in the different lines and continua, and statistical equilibrium of level populations. These parameters vary with the radial coordinate r. The numerical solution of these equations, in the case of a cylindrical geometry, has been described in Paper I and is not reproduced here. These computations produce absorption coefficients, source functions, and intensities in different transitions, which allow the determination of $E_{\rm rad}$, according to Eq. (7). Internal energy U may be obtained from physical variables and hydrogen level populations, using Eqs. (2) to (4). The ratio of the two quantities gives $t_{\rm CV}$. Since the present models satisfy SE equations, $t_{\rm CP}$ differ from $t_{\rm CV}$ by a multiplicative constant, so it will be sufficient to use $t_{\rm CV}$ for the present discussion.

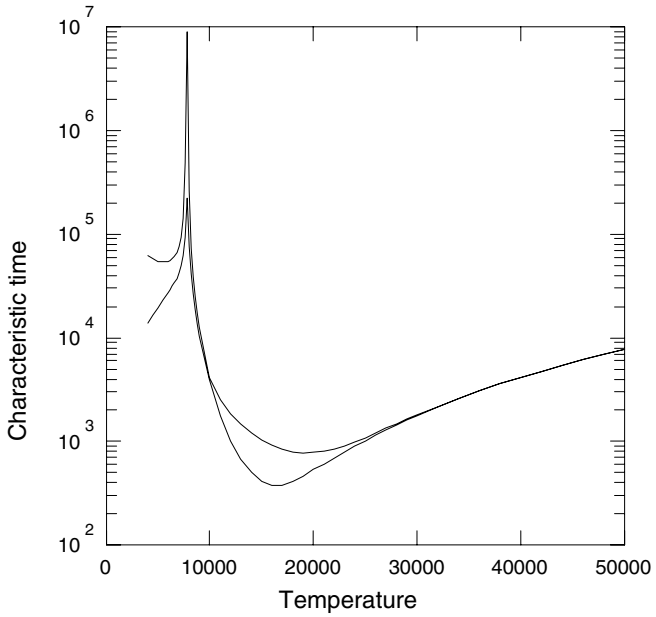

Fig. 1. Variations of the minimum and maximum of t_{CV} (s) vs. T (K), other physical parameters being set to standard values.

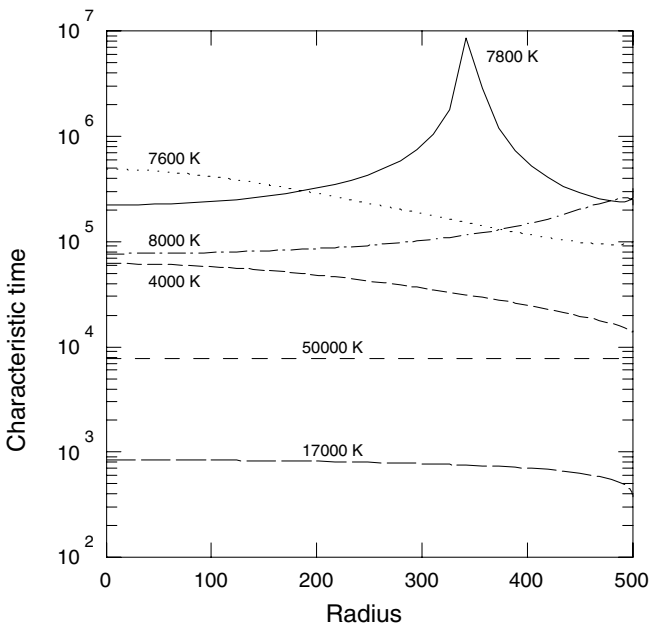

Fig. 2. Variations of t_{CV} (s) vs. r (km), for a sample of temperatures ranging from 4000 to 50 000 K.

3.1. Effect of temperature

The numerical values of t_{CV} have been computed for a series of models with temperatures ranging from 4000 to 50 000 K. The other physical parameters were taken as constant: P = 0.1 dyn cm^{-2}, D = 1000 km, ξ = 5 km s^{-1}, and $H = 10^4$ km. The relaxation time is also a function of the distance r to the axis of the cylinder. For each model, we have taken the minimum and the maximum of t_{CV} along r, and plot them vs. temperature in Fig. 1. The two curves present a peak around 7800 K and a minimum between 15 000 and 20 000 K. The peak near 7800 K indicates that the cylinder at this temperature is close to radiative equilibrium. The sign of E_{rad}, not visible in Fig. 1, is positive for temperatures lower than 7800 K and negative on the other side of the peak. The increase of t_{CV} at temperatures higher than 20 000 K means than U grows more rapidly than $|E_{rad}|$ at high temperatures.

Figure 2 represents the variation of t_{CV} along the radius of the cylinder for a sample of temperatures. All curves are monotonic, except the one corresponding to 7800 K, which presents a peak. So, for this temperature, there is a position inside the cylinder where the matter is in thermal equilibrium. Inside this position, E_{rad} is negative, and positive outside. At lower temperatures (4000 to 7600 K), t_{CV} decreases towards the exterior, while it increases at slightly higher temperatures (8000 K). At high temperatures, the variation of t_{CV} vs. r becomes very flat, since the decrease of optical thicknesses in all transitions tends to make the medium more and more homogeneous.

3.2. Effect of pressure

Now, we fix the temperature and allow the pressure to vary. Other parameters are set to their standard values: D = 1000 km, H = 10 000 km, and ξ = 5 km s^{-1}. The variations of t_{CV} with pressure appear to be quite different at high and low temperatures. At temperatures high enough with respect to the mean radiative equilibrium value (7800 K), t_{CV} decreases regularly with pressure. For instance, at 10 000 K (Fig. 3), t_{CV} decreases from 3×10^5 s at 0.01 dyn cm^{-2} to 4×10^3 s at 0.1 dyn cm^{-2} to about

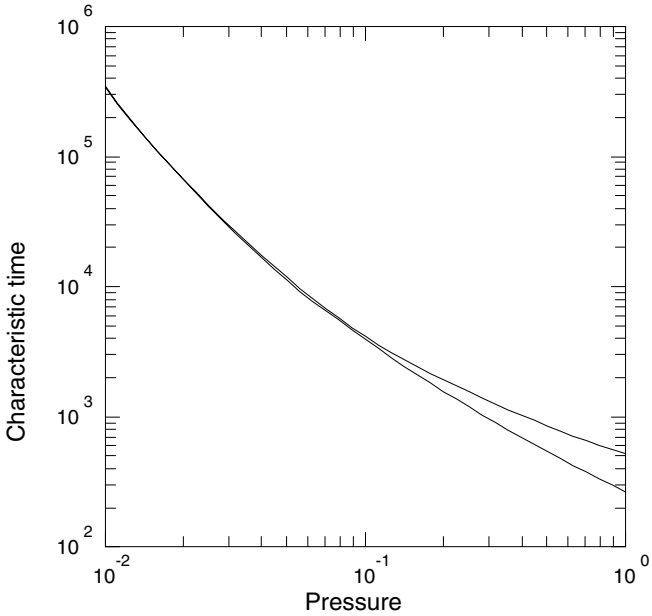

Fig. 3. Variations of the minimum and maximum of t_{CV} (s) vs. P (dyn cm^{-2}), for T = 10 000 K, D = 1000 km, and H = 10 000 km.

300 s at 1 dyn cm^{-2}. In this case, E_{rad} is always negative, and there is little variation along the radius of the cylinder. The decrease of t_{CV} with pressure is principally due to the increase of collisions that produce a more efficient transfer of energy between matter and radiation, so that the gas cools more rapidly.

The variation of t_{CV} is more complicated for low temperatures (T < 8000 K) since, for pressures high enough, E_{rad} changes sign along the radius of the cylinder. For example, in Fig. 4 we have plotted the variation of E_{rad}/U (whose absolute value is the inverse of t_{CV}) along the radius for T = 7000 K and different pressures. At low pressures (0.01 to 0.1 dyn cm^{-2}), E_{rad} is always positive along the radius. At higher pressures, E_{rad} is negative near the axis and positive near the surface. When the

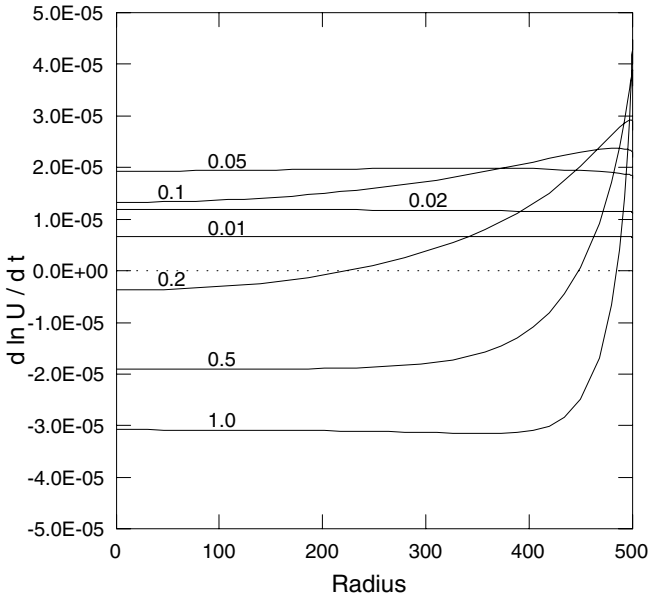

Fig. 4. Ratio of net energy gain to internal energy vs. r (km), for a sample of models with $T = 7000$ K and different pressures from 0.01 to 1 dyn cm^{-2}. Variations of $E_{\rm rad}/U = {\rm d}\ln U/{\rm d}t$ are represented by full lines, labeled with the values of pressure. The dotted line shows the position of radiative equilibrium ($E_{\rm rad} = 0$).

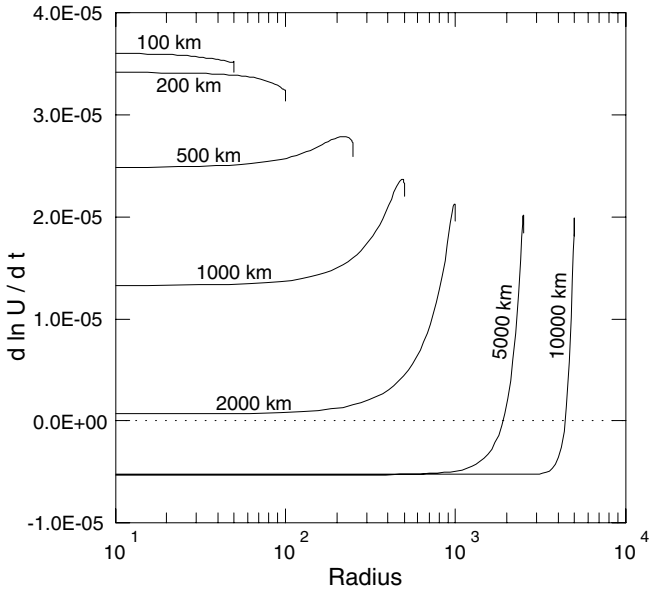

Fig. 5. Variations of $E_{\rm rad}/U$ for different diameters of the cylinder, from 100 to 10 000 km. Other physical parameters are: $T = 7000$ K, $P = 0.1$ dyn cm^{-2}, $\xi = 5$ km s^{-1}, and $H = 10\,000$ km.

pressure grows, the point where $E_{\rm rad}$ changes sign moves closer to the surface.

3.3. Effect of other parameters

The diameter of the cylinder is also an important parameter for the thermal balance of the matter inside the structure. Its effect may be compared to that of pressure, since both parameters tend to increase the optical thickness of the object in the different transitions of hydrogen. However, the change of diameter has little effect on collisional transition rates, contrary to pressure, so that the results may be somewhat different. For $T = 10\,000$ K and $P = 0.1$ dyn cm^{-2}, $E_{\rm rad}$ remains negative whatever the value of the diameter between 100 and 10 000 km, as in the case of pressure variations. However, the variation of $t_{\rm CV}$ vs. D is very flat in this case, remaining in the range of 4000 to 6000 s. For $T = 7000$ K, we have, as in the case of pressure variations, a possibility of a change of sign for $E_{\rm rad}$, provided that D is large enough. As shown by Fig. 5, $E_{\rm rad}$ is uniformly positive for $D \leq 2000$ km. For 5000 and 10 000 km, $E_{\rm rad}$ is negative near the axis of the cylinder and positive near the surface.

The last parameter examined here is the altitude H of the object above the solar surface. Its effect consists of changing the incident intensities at the surface of the cylinder. So, the preceding results are not qualitatively modified by the variations of H, but, quantitatively, the temperature of radiative equilibrium is somewhat lowered as H increases. For instance, the peak of $t_{\rm CV}(T)$, which is encountered near $T = 7800$ K when the altitude is 10 000 km, is shifted close to 7600 K for $H = 50\,000$ km.

4. Radiative equilibrium models

The computations of the preceding section show that, in the absence of any internal source of energy, isothermal models are in thermal unbalance. Then, the parameter ${\rm d}T/{\rm d}t$, given by Eq. (25) in the case of constant pressure, indicates the rate of spontaneous change of temperature for each region of the cylinder. If we allow the temperature to vary, while keeping the other parameters (P, D, ξ, H) constant, we have a means of computing radiative equilibrium models.

4.1. Spontaneous evolution of temperature

The problem is treated by an initial-value method. The parameters P, D, ξ, and H are fixed to the chosen values and, at time $t = 0$, the temperature is fixed to an arbitrary value T_0. The method consists of successively increasing the time by a small quantity Δt and changing the temperature T_i, at position r_i, to $T_i + \Delta T_i$ with

$$\Delta T_i = \left(\frac{{\rm d}T_i}{{\rm d}t}\right)_P \Delta t, \tag{29}$$

which is simply the Newton method. The system is assumed to be constantly in statistical equilibrium, which constitutes some kind of quasi-static approximation. This approximation seems reasonable for discrete transitions, the timescales associated with these transitions being shorter than 1 s. The recombination rates for the Lyman continuum, for the present models, are generally in the range $[10^{-4}, 10^{-2}]$ s^{-1}, depending on temperature and pressure. So, in some cases, the evolution may be slower than expected from the quasi-static approximation. Further computations including the dynamics of hydrogen level populations will be necessary to clarify this point. However, this problem does not affect the final result, i.e. the structure of the radiative equilibrium model. With the set of temperatures so obtained, we simultaneously solve the equation of radiative transfer, statistical equilibrium, and electric neutrality to obtain a new set of physical parameters and new values of $({\rm d}T_i/{\rm d}t)_P$. Then, we iterate on temperatures until $E_{\rm rad}$ becomes low enough or, equivalently, until $t_{\rm CV}$ becomes larger than a given criterion. In the present case, we have chosen the criterion $t_{\rm CV} > 10^9$ s. Since statistical

equilibrium is assumed, the temperature derivative (25) reduces to

$$\left(\frac{\mathrm{d}T}{\mathrm{d}t}\right)_P = \frac{2}{5}\frac{E_{\rm rad}}{n_{\rm H}\,(1+A_{\rm He}+y)\,k}. \quad (30)$$

The method is found to be convergent for all the models under study, provided that the time increments are small enough. The time step is chosen as the minimum of two quantities. The first one is a constant value that is effective close to the equilibrium, and is necessary to avoid oscillations of temperature near the surface. It is taken to be equal to 1000 s in most cases (500 s in a few cases). The other limiting quantity is effective when the changes of temperature are fast. A value equal to 1% of $t_{\rm CV}$ (minimum taken along the radius) is found to be adequate.

The system of equations is nonlinear: in particular, the coefficients of radiative transfer equations depend on absorption coefficients, which in turn depend on level populations that are the solutions of equations. As a consequence, the uniqueness of the solution (i.e., the temperatures of the final model) is not certain. However, in the cases presently studied, it is empirically found that, for a given set of parameters (P, D, ξ, H), the final temperature is the same, whatever the initial temperature is. As an example, in Fig. 6 we show the results obtained with the model (P = 0.1 dyn cm^{-2}, D = 1000 km, ξ = 5 km s^{-1}, H = 10 000 km) for three initial temperatures: 4000, 10 000, and 30 000 K. Figure 6a shows the evolution of temperatures along the axis and at the surface of the cylinder. The radiative equilibrium temperature is reached more rapidly near the surface than in the interior, and is achieved in a few hours for the model under consideration. The evolution from a low initial temperature is slower than that from higher temperatures. This is a consequence of lower hydrogen ionization at low temperatures, which acts in two different ways. First, it increases the optical thicknesses in Lyman lines and continuum, which contributes to the thermal insulation of the cylinder core. Second, the lower electron density results in lower collisional transition rates, and thus reduces exchanges of energy between matter and radiation. This slower evolution is also visible on the variation of $t_{\rm CV}$ vs. time, which is shown in Fig. 6b. Whatever the initial temperature, the final temperatures are the same (Fig. 6c), and correspond to radiative equilibrium.

4.2. The case of thick models

As expected from considerations on optical thicknesses in Lyman lines, models with large diameters and high pressures evolve more slowly. For example, we examine the case (P = 1 dyn cm^{-2}, $D = 10^4$ km, ξ = 5 km s^{-1}, H = 10 000 km) evolving from two initial temperatures: 5000 and 10 000 K. Figure 7 shows the variations of temperatures with time, either along the axis or at the surface. Radiative equilibrium is reached at the surface in a time of the order of 1 h. On the contrary, the evolution is very slow along the axis, and the final temperature is reached, within 1 K, after about 10^6 s, i.e., 10 days. The difference between instantaneous and final temperatures, along the axis, is represented in Fig. 7b. As previously noticed, the evolution from the lower initial temperature (5000 K) is slower than that corresponding to the higher temperature (10 000 K). The consequence of this slow evolution inside thick and cool structures is the possibility of observing such condensations of matter even if they are at a temperature substantially different from that corresponding to radiative equilibrium. This may be useful for the understanding of the prominence–filament phenomenon.

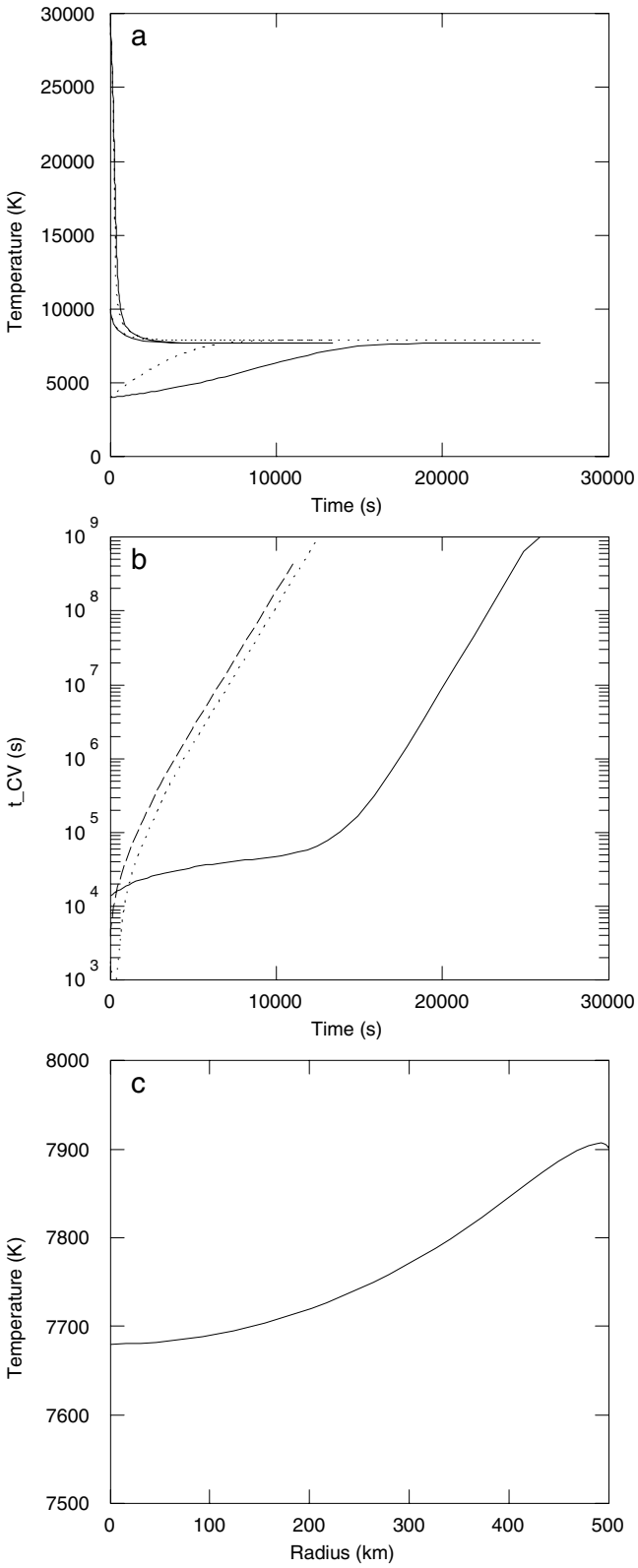

Fig. 6. Temporal evolution for the standard model (P = 0.1 dyn cm^{-2}, D = 1000 km, ξ = 5 km s^{-1}, H = 10 000 km). **a)** variation of temperature with time, from three different initial temperatures: 4000, 10 000, and 30 000 K. Full lines: temperatures along the axis of the cylinder; dotted lines: surface temperatures. **b)** variation of $t_{\rm CV}$ (minimum along the radius) with time. Full line: from initial temperature 4000 K; dashed line: from 10 000 K; dotted line: from 30 000 K. **c)** final temperature (independent of initial temperature) vs. r.

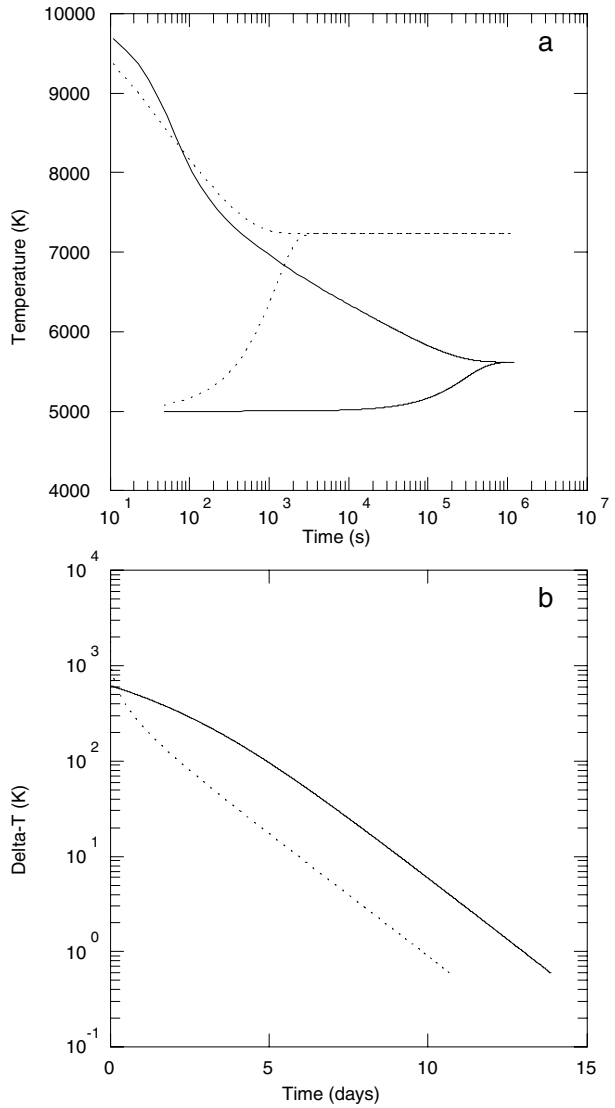

Fig. 7. Temporal evolution for a thick model (P = 1 dyn cm^{-2}, D = 10 000 km, ξ = 5 km s^{-1}, H = 10 000 km), from two different initial temperatures: 5000 and 10 000 K. **a)** Variations of axis (full lines) and surface (dotted lines) temperatures vs. time. **b)** Absolute difference between the temperature at time t, along the axis, and its final value; full line: evolution from 5000 K; dotted line: evolution from 10 000 K.

4.3. Final models

The radiative equilibrium models may be obtained in every case by following the natural evolution of temperature as previously described. However, in the case of thick models, this procedure may require several thousands of iterations. In this case, it is much faster to proceed by successive interpolations. The radial grid ($r_i; i = 1, \ldots, N$) is kept constant during the computation, as well as the pressure and other physical parameters, except temperature. For a given distribution of temperature ($T_i; i = 1, \ldots, N$), we can obtain a distribution of radiative gains $E_{\rm rad}(i); i = 1, \ldots, N$) by solving the radiative transfer and statistical equilibrium (RTSE) equations. The aim of the method is to find the distribution of T that minimizes $E_{\rm rad}$. For this purpose, we consider a set of M models, each one being identified by the index (j; $j = 1, \ldots, M$). So, a set of models is defined by a 2D array T_{ij}. By solving the RTSE equations for each model, we obtain another 2D array $E_{ij} = E_{\rm rad}(T_{ij})$. The interpolation method proceeds as follows:

1. At the beginning, we choose a set of isothermal models ($T_{ij} = T_{0j}, \forall i, \forall j$). Temperatures are taken in decreasing order ($T_{01} > T_{02} > \cdots > T_{0M}$) so that, for any given position r_i, the corresponding E_{ij} are in increasing order ($E_{i1} < E_{i2} < \cdots < E_{iM}$). In addition, the range of temperatures must be large enough so that $E_{\rm rad}$ can be uniformly negative for model 1 and positive for model M. The temperatures of two successive models differ by a given quantity ΔT. For instance, for M = 11, we may use T_{01} = 10 000 K and T_{0M} = 5000 K, so that ΔT = 500 K.
2. At a stage of iteration, we have a temperature array T_{ij} and the resulting array E_{ij}. For each position r_i, we consider a function $y(x)$ that goes through the M points ($x_j = E_{ij}; y_j = T_{ij}; j = 1, \ldots, M$). By interpolation, we obtain the value of y corresponding to $x = 0$. This value $y(0)$ is used to form a new guess of the temperature distribution $T_i(r_i)$. Once this process is completed for all positions r_i, the RTSE equations are solved for the new temperature distribution to get the radiative terms E_i. If these radiative terms satisfy a given convergence criterion (e.g., $|E_i|/U_i < 10^{-9}$ s^{-1}, $\forall i$), the temperature distribution $T_i(r_i)$ is considered as the "radiative equilibrium model".
3. If the convergence criterion is not satisfied, we define a new set of M models centered on the temperature distribution $T_i(r_i)$. The temperature step ΔT is reduced with respect to the preceding value (for instance, if M = 11, ΔT may be divided by 5) and we set

$$T_{ij} = T_i + \left(\frac{M+1}{2} - j\right)\Delta T, \forall i, \forall j,$$

and start process (2) again.

There is some arbitrariness in the choice of parameters M and ΔT, but, in practice, this process works well and the radiative equilibrium model is obtained in a few iterations.

A series of radiative equilibrium models has been computed for 7 pressures (0.01, 0.02, 0.05, 0.1, 0.2, 0.5, and 1 dyn cm^{-2}) and 7 diameters (100, 200, 500, 1000, 2000, 5000, and 10 000 km), ξ = 5 km s^{-1} and H = 10 000 km. In addition, a few models, corresponding to the mean pressure, diameter, and microturbulent velocity, have been computed for different altitudes up to 90 000 km. These 53 models are tabulated in an ASCII file available on the web at the following address: `http://www.ias.u-psud.fr/gouttebroze/rtcy4rem.dat/`. This table includes the following parameters for each model, as a function of r (km): T, ρ, y, U, and the residual value of $E_{\rm rad}$. The variations of temperature along the radius are represented in Fig. 8 for two diameters, 200 and 5000 km, representative of thin and thick models, respectively. In both cases, low pressure models are almost isothermal and exhibit relatively high temperatures. For a diameter of 200 km, radiative equilibrium models remain quasi-isothermal up to P = 0.2 dyn cm^{-2}. For the two remaining models, a positive gradient of temperature appears between the axis and the surface. The mean temperature of the models decreases regularly with pressure. The large diameter models (D = 5000 km) exhibit a similar behavior, but the two lowest pressures only produce quasi-isothermal structures. Models with pressure $\geq$ 0.1 dyn cm^{-2} possess a cool core with a temperature lower than 6000 K. For all models, there is a correlation between temperature and ionization, which is illustrated by Fig. 9. In this figure, we have plotted the different relations $y(T)$ corresponding

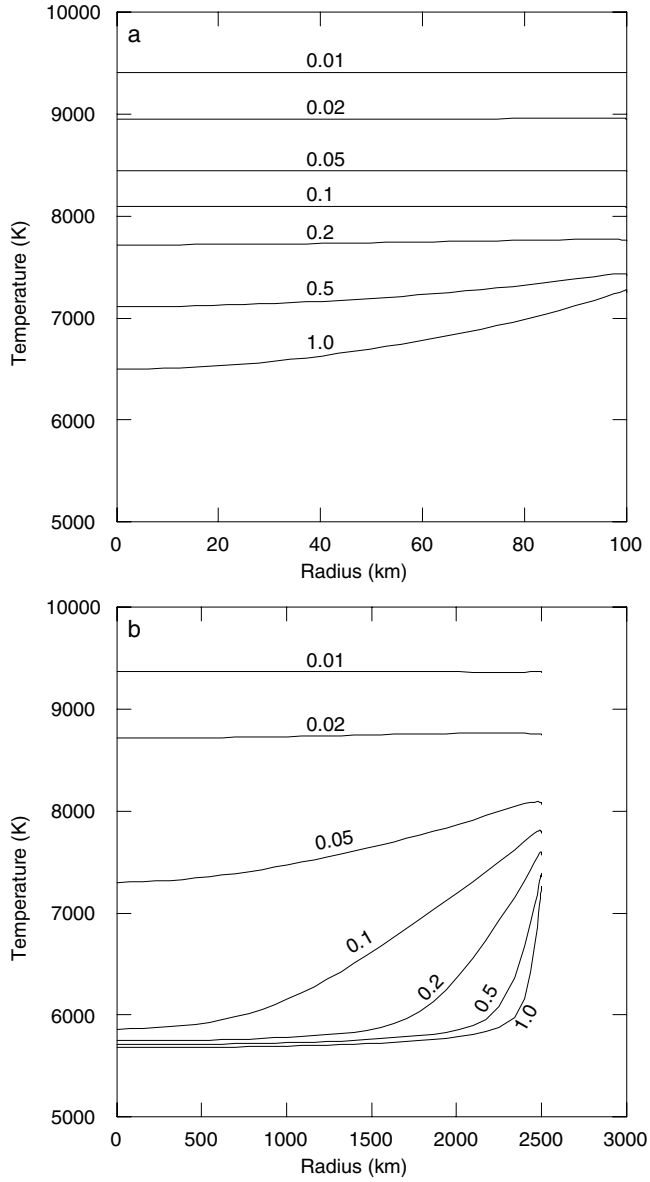

Fig. 8. Temperature variation along the radius for models in radiative equilibrium for two diameters and different pressures. Pressures (in dyn cm^{-2}) are indicated as curve labels. **a)** D = 200 km. **b)** D = 5000 km.

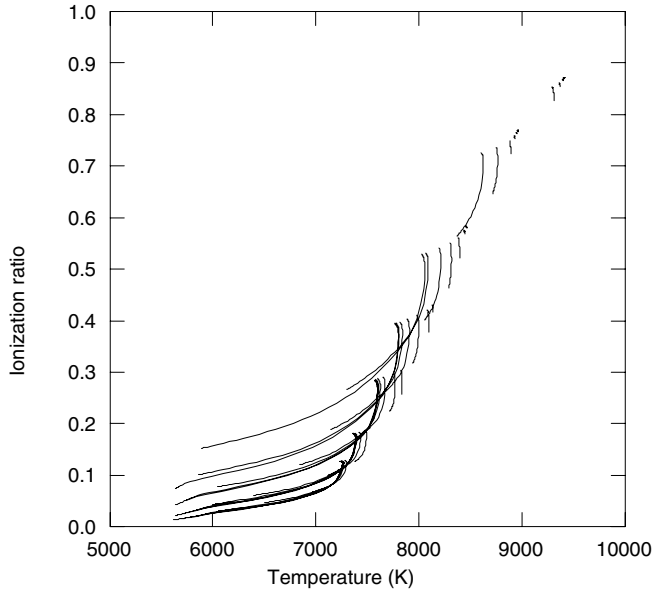

Fig. 9. Ionization-temperature correlation for models in radiative equilibrium. The relation $y(T)$ is plotted for the different models with $H = 10^4$ km.

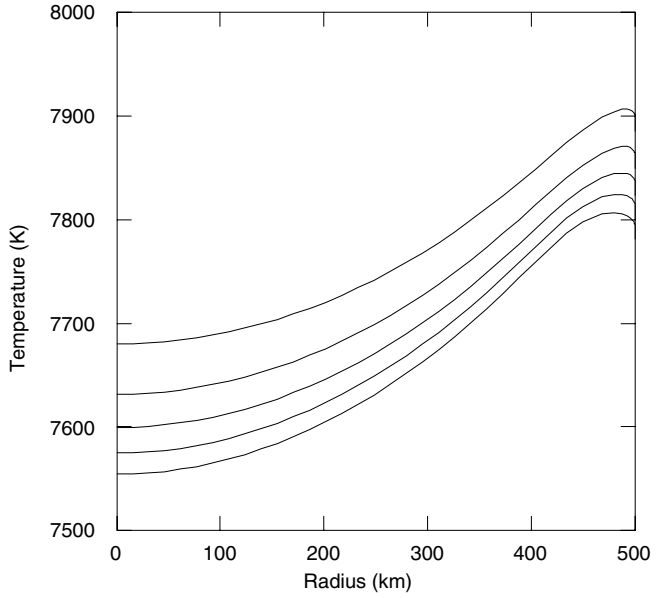

Fig. 10. Temperature variation along the radius for the standard model (P = 0.1 dyn cm^{-2}, D = 1000 km, and ξ = 5 km s^{-1}) and different altitudes: H = 10 000, 30 000, 50 000, 70 000, and 90 000 km. Each curve corresponds to one altitude and T decreases when H increases.

to the 49 models with H = 10 000 km. The thinnest models are practically reduced to a point, since both y and T are almost constant along the radius. For thick models, the shape of the curves indicates that y increases rapidly near the surface, as a result of photoionization by the incident Lyman continuum.

To study the influence of altitude, we have computed radiative equilibrium models for a given set of physical parameters (P = 0.1 dyn cm^{-2}, D = 1000 km, and ξ = 5 km s^{-1}) and different altitudes ranging from 10^4 to 9×10^4 km. The energy input regularly decreases when H increases, so that the equilibrium temperature is progressively shifted toward lower values. This effect is represented quantitatively in Fig. 10.

4.4. Stability

With the present notations, the condition for the thermal equilibrium to be stable is

$$\frac{\mathrm{d}E_{\mathrm{rad}}}{\mathrm{d}T} < 0. \tag{31}$$

However, this formula is not sufficient in itself and it is necessary to define how the medium reacts to a variation of temperature. Parker (1953), in his early analysis of the problem, considered constant density (frozen) matter. Later on, Field (1965) and Defouw (1970) treated the problem in the framework of constant pressure transformations. This is also the point of view adopted here. Defouw gave a fully analytic treatment of instability, but

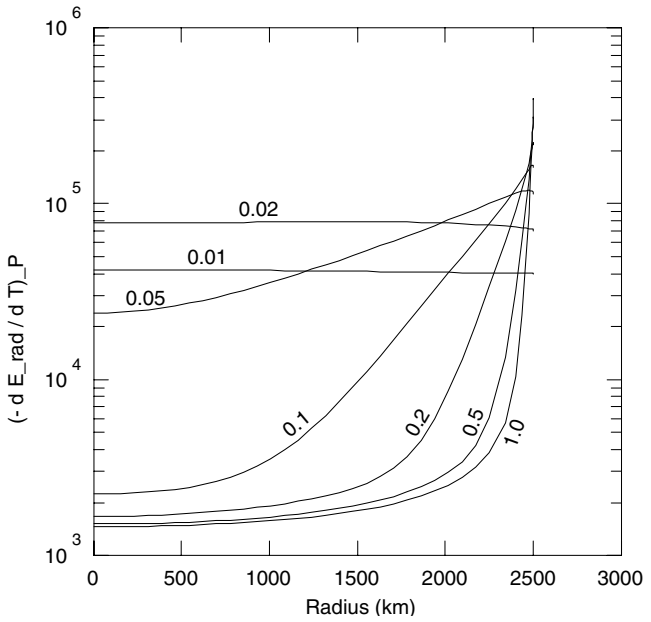

Fig. 11. Variation of the stability criterion $(-\partial E_{\rm rad}/\partial T)_P$, in erg g^{-1} s^{-1} K^{-1}, along the radius for models in radiative equilibrium with D = 5000 km and different pressures. Pressures (in dyn cm^{-2}) are indicated as curve labels.

restricted to a simplified hydrogen atom with one bound level plus continuum. The medium was assumed to be optically thin. He concluded that plasmas were thermally stable under a transition temperature of about 17 500 K, and unstable above. We have numerically computed the isobaric derivative $(\partial E_{\rm rad}/\partial T)_P$ for all our radiative equilibrium models. Since most of these models are optically thick in Lyman lines and continuum, $(\partial E_{\rm rad}/\partial T)_P$ is also a function of the radial coordinate r. It is found that $(\partial E_{\rm rad}/\partial T)_P$ is negative for all models and all values of r, which means that they are thermally stable. Since all temperatures are lower than 10 000 K, this result is in agreement with Defouw's criterion. The stability factor $(-\partial E_{\rm rad}/\partial T)_P$ is plotted vs. r in Fig. 11 for models with D = 5000 km and different pressures. At very low pressures, models are close to the optically thin case, so that the stability factor is practically constant. At high pressures, it varies by more than two orders of magnitude between the axis and the surface. The small value of the stability factor near the axis is related with the very slow rate of thermal evolution in the core of thick models, as was stressed in Sect. 4.2.

5. Conclusion

The thermal evolution and equilibrium of filamentary structures observed in the solar atmosphere has been investigated using 1D cylindrical models and non-LTE radiative transfer techniques. The radiative gains and losses have been computed for each transition of the hydrogen atom and their sum $E_{\rm rad}$ compared to the internal energy U. In this way, we obtained the time derivatives of temperature, corresponding to either isochoric or isobaric evolution. The isobaric derivative was used to compute the spontaneous evolution of structures toward a final radiative equilibrium model. Two different types of evolution may be distinguished: Thin models (small diameter, low pressure) evolve rapidly and produce final radiative equilibrium models with quasi-constant and relatively high temperature. Thick models (large diameter, high pressure) evolve very slowly near the axis. Their final state consists of a cool core ($T < 6000$ K), weakly ionized, and steep gradients of temperature and ionization near the surface. The slow evolution of temperatures of thick cylinders near the axis results in the probability of observing substantial departures from thermal equilibrium there. Radiative equilibrium models are found to be stable in the whole range of physical parameters investigated.

Further developments seem to be necessary in the future. First, the statistical equilibrium assumption should be validated by a study of the dynamics of hydrogen level populations. Second, the introduction of conductivity would be necessary to produce a transition region between the cylinder and the coronal medium. Other important improvements are also envisaged: introduction of helium, partial frequency redistribution in Lyman lines, and 2-dimension radiative equilibrium.

References

Anderson, L. S. 1989, ApJ, 339, 558
Auer, L. H., & Mihalas, D. 1969, ApJ, 158, 641
Bonnet, R. M., Bruner, E. C. Jr, Acton, L. W., Brown, W. A., & Decaudin, M. 1980, ApJ, 237, L47
Defouw, R. J. 1970, ApJ, 161, 55
Field, G. B. 1965, ApJ, 142, 531
Fontenla, J. M., & Rovira, M. 1983, Sol. Phys., 85, 141
Fontenla, J. M., & Rovira, M. 1985, Sol. Phys., 96, 53
Gouttebroze, P. 2004, A&A, 413, 733 (Paper I)
Gouttebroze, P. 2005, A&A, 434, 1165 (Paper II)
Gouttebroze, P. 2006, A&A, 448, 367 (Paper III)
Heasley, J. N., & Mihalas, D. 1976, ApJ, 205, 273
Hopf, E. 1934, Mathematical Problems of Radiative Equilibrium (Cambridge University Press)
Mihalas, D. 1967, in Methods in Computational Physics, vol. 7, ed. B. Alder, S. Fernbach, & M. Rotenberg (New York: Academic Press), 1
Milne, E. A. 1921, MNRAS, 81, 361
Parker, E. N. 1953, ApJ, 117, 431
Vourlidas, A., Klimchuk, J. A., Korendyke, C. M., Tarbell, T. D., & Handy, B. N. 2001, ApJ, 563, 374